Bulgakova et al., http://www.jcb.org/cgi/content/full/jcb.201211159/DC1

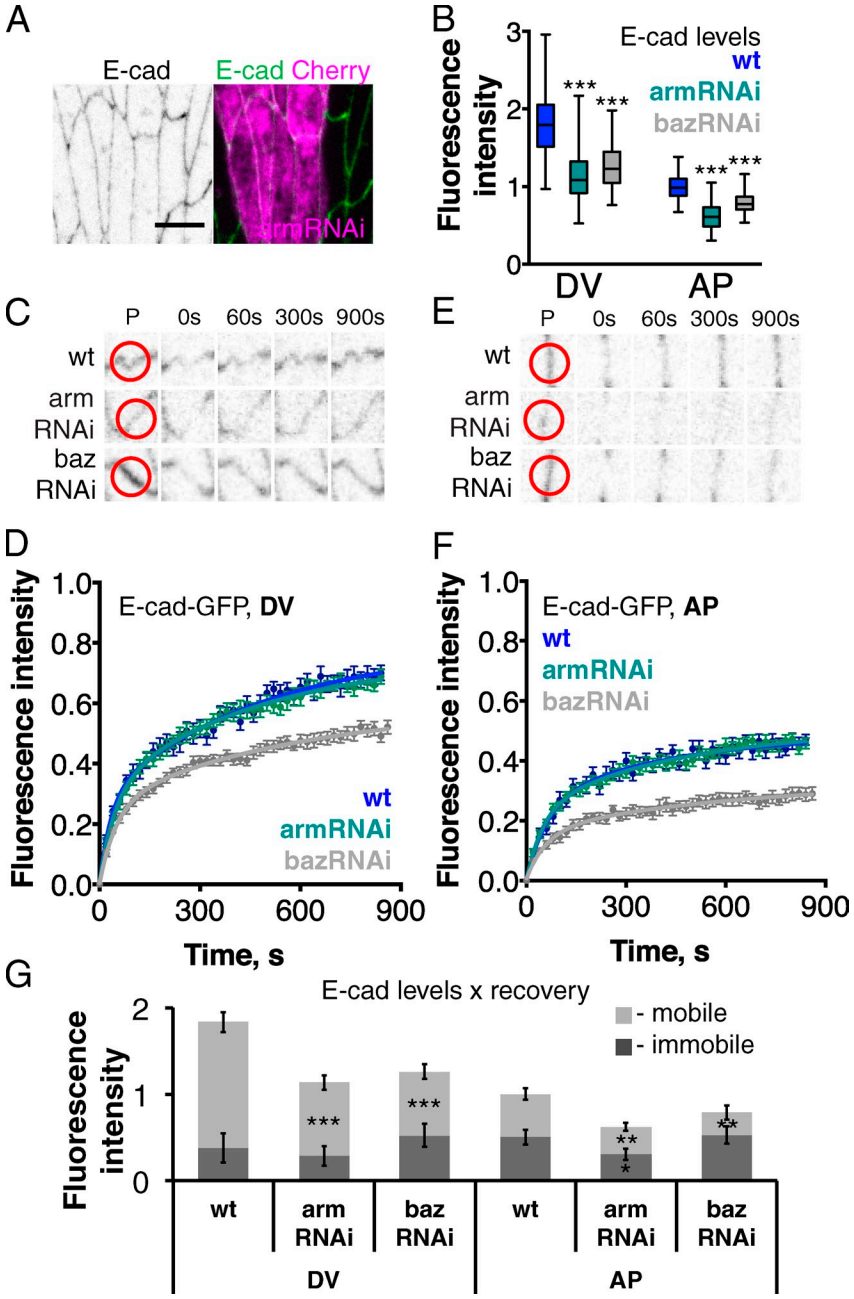

Figure S1. **Down-regulation of β-catenin (arm) reduces mobile and immobile pools of E-cad.** (A) E-cad localization in cells expressing *armRNAi* (anti–E-cad, black/green; Cherry-tagged products in experimental cells, magenta) and (B) quantification of junctional E-cad levels in wild type, *armRNAi*, and *bazRNAi*. Bar, 5 µm. (C–F) Recovery of E-cad in cells that express *armRNAi* or *bazRNAi* at the DV borders (C and D) and AP borders (E and F) with examples of recovery in C and E, with red circles on the prebleached frame (P) showing the bleach spots, and averaged recovery curves (error bars indicate mean ± SEM) in D and F. (G) Combining the recovery and E-cad levels gives an estimate of mobile and immobile E-cad pools (mean ± SEM) at DV and AP borders when *armRNAi* or *bazRNAi* was expressed. The *bazRNAi* data are the same as shown in Fig. 3. Table S1 has detailed numbers for this and all other figures. *, $P < 0.01$; **, $P < 0.001$; ***, $P < 0.0001$.

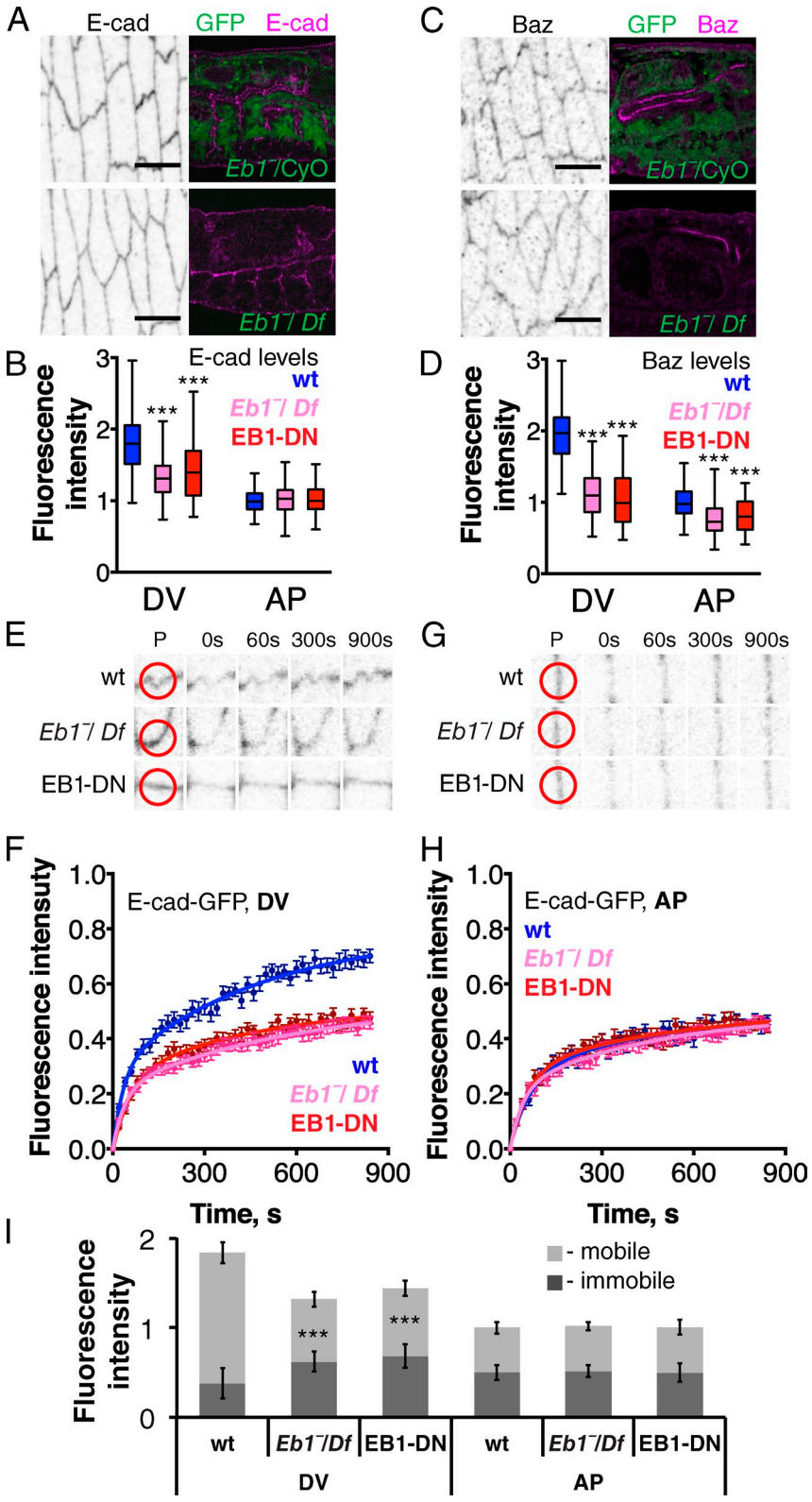

Figure S2. ***Eb1* mutants and EB1-DN cause similar changes to E-cad distribution and dynamics.** (A–D) Endogenous E-cad (A) and Baz (C) localization in embryos heterozygous for *Eb1* (*Eb1*$^{-}$/*CyO*) and zygotic *Eb1* mutant (*Eb1*$^{-}$/*Df*; anti–E-cad, black/magenta in A; anti-Baz, black/magenta in C; the right panels in A and C show overviews of embryos demonstrating how we distinguished between mutant and control embryos using balancer chromosome carrying GFP and wild-type copy of *Eb1*, green), and quantitation of E-cad (B) and Baz (D) levels at the junctions. The data for EB1-DN expression from Fig. 6 is included for comparison. Bars, 10 µm. (E–H) FRAP of E-cad–GFP in *Eb1* zygotic mutant embryos, compared with wild type or EB1-DN at DV (E and F) and AP borders (G and H), with examples of recovery in E and G, with red circles on the prebleached frame (P) showing the bleach spots, and averaged recovery curves (mean ± SEM) in F and H. (I) Combining the recovery and E-cad levels gives an estimate of mobile and immobile E-cad pools (error bars indicate mean ± SEM). ***, $P < 0.0001$.

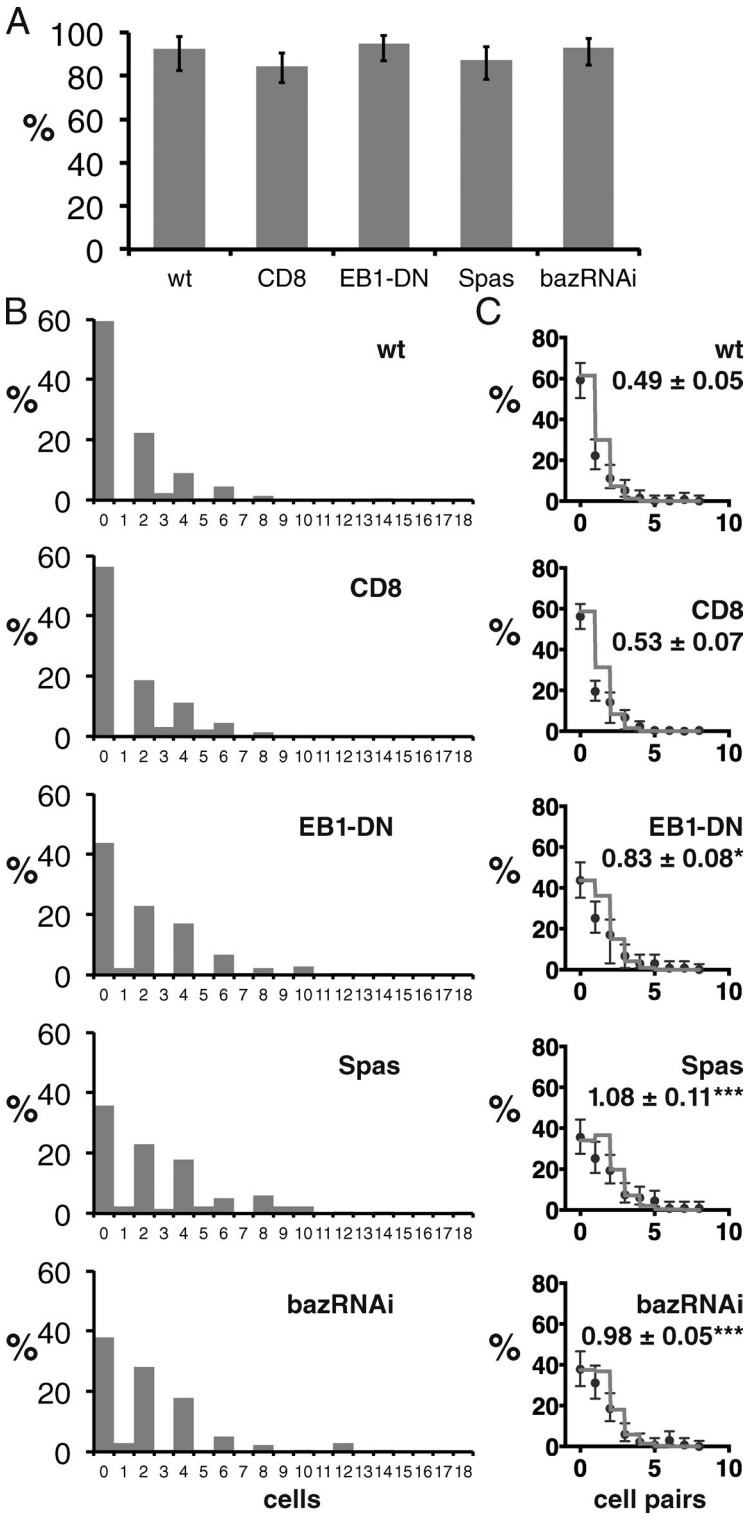

Figure S3. **Cells cross the segment boundary in pairs at a steady rate.** For each posterior compartment stripe of cells, we counted the cells that had crossed the segment border and still expressed *en::Gal4*–driven GFP. (A) Cells that had crossed the boundary were found in even numbers. "%" refers to the percentage of those stripes where some cells had crossed and the number of crossed cells was even (error bars indicate mean ± 95% CI). We compared stripes with no additional construct expressed (wt) to those coexpressing CD8, EB1-DN, Spas, or *baz-RNAi*. (B) Perturbing mobile E-cad increases the number of crossing events. "%" is the percent of stripes showing x cells that had crossed the boundary in wild type (expression of GFP only) and with expression of CD8, EB1-DN, Spas, or *baz-RNAi*. The data are from three stripes per embryo (segments A1–A3) from the following number of embryos: $n = 45$ for wild type, EB1-DN, Spas, or *baz-RNAi*; and $n = 90$ for CD8. (C) Numbers of crossed cell fits with a steady rate of crossing of cell pairs. "%" in this case shows the percentage of stripes with x pairs of cells that had crossed the boundary. We fitted the data in B using the probability mass function of Poisson distribution, $F(k) = \lambda^k \times e^{-\lambda}/k!$, where k is number of cell pairs that had crossed the boundary, and we seek to determine λ, the weighted mean of the crossing rate of cell pairs. The fitting was performed with Prism software entering the above equation as a user-defined equation for nonlinear regression for integer k, ranging from 0 to 8. Including higher values of k did not change the best fit parameter λ. The best fit (gray line) and the best fit parameter λ (mean ± SEM) are shown for stripes with no additional construct expressed (wt) and those coexpressing CD8, EB1-DN, Spas, or *baz-RNAi*. Deviation of the data from the Poisson distribution model was tested in Prism with Runs Test, and there was no significant deviation. The significance of the difference between the best fit λ parameters between the treatments that reduce E-cad–Baz and controls was calculated using the extra sum-of-squares F-test in Prism, and is indicated both here and in Fig. 6 B (*, $P < 0.01$; ***, $P < 0.0001$).

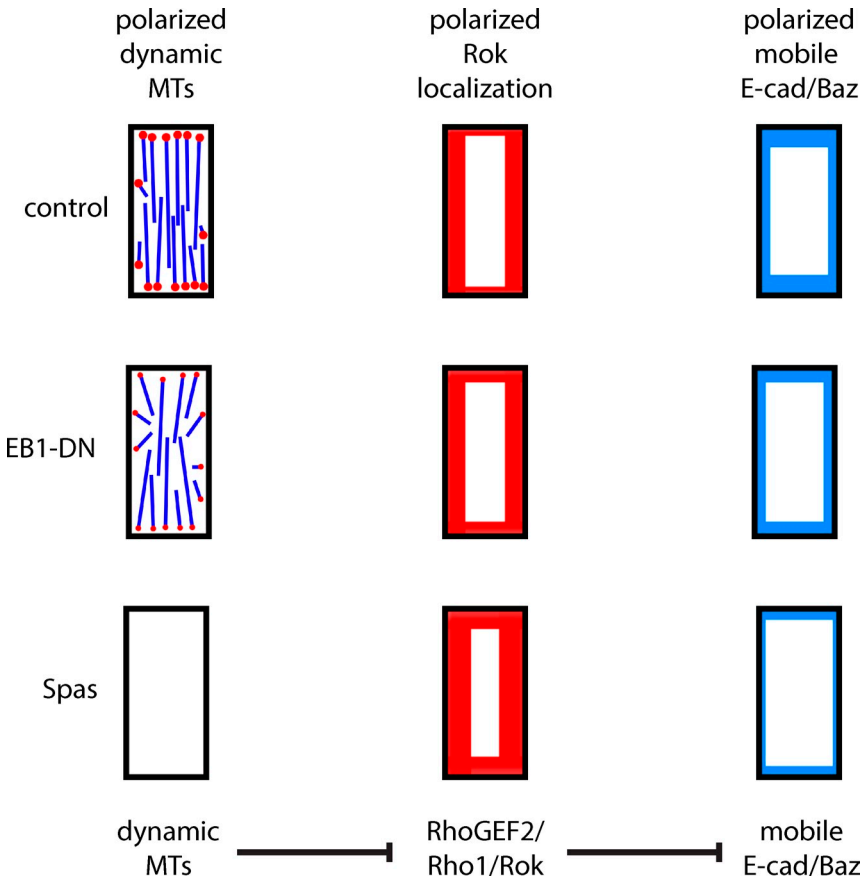

Figure S4. **Model of regulation of mobile E-cad distribution by dynamic MTs with the changes caused by EB1-DN and Spas diagrammed.** For more details see Fig. 10 and the main text.

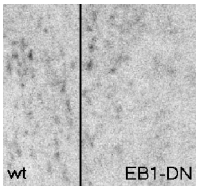

Video 1. **Epidermis at stage 15 of embryo development expressing EB1-GFP (black) tracking MT plus ends in control (left) and cells expressing EB1-DN (right).** Images were analyzed by time-lapse microscopy using spinning disc confocal microscope (Eclipse Ti-E inverted microscope [Nikon], equipped with a CFI Apochromat TIRF 100× 1.49 NA oil objective lens [Nikon] and a motorized CSU-X1-A1 confocal head [Yokogawa Corporation of America]). Frames were taken every 0.5 s for 50 s.

Table S1 gives numerical values of protein accumulation at cell borders and best-fit parameters for FRAP experiments, and is available for download as a Microsoft Excel file.